

THE EFFICIENCY OF RESONANT RELAXATION AROUND A MASSIVE BLACK HOLE

EHUD EILON¹, GÁBOR KUPI AND TAL ALEXANDER²

Weizmann Institute of Science, Rehovot 76100, Israel

Draft version October 30, 2018

ABSTRACT

Resonant relaxation (RR) is a rapid relaxation process that operates in the nearly-Keplerian potential near a massive black hole (MBH). RR dominates the dynamics of compact remnants that inspiral into a MBH and emit gravitational waves (extreme mass ratio inspiral events, EMRIs). RR can either increase the EMRI rate, or strongly suppress it, depending on its still poorly-determined efficiency. We use small-scale Newtonian N -body simulations to measure the RR efficiency and to explore its possible dependence on the stellar number density profile around the MBH, and the mass-ratio between the MBH and a star (a single-mass stellar population is assumed). We develop an efficient and robust procedure for detecting and measuring RR in N -body simulations. We present a suite of simulations with a range of stellar density profiles and mass-ratios, and measure the mean RR efficiency in the near-Keplerian limit. We do not find a statistically significant dependence on the density profile or the mass-ratio. Our numerical determination of the RR efficiency in the Newtonian, single-mass population approximations, suggests that RR will likely *enhance* the EMRI rate by a factor of a few over the rates predicted assuming only slow stochastic two-body relaxation.

Subject headings: black hole physics—galaxies: nuclei—stars: kinematics and dynamics—gravitational waves

1. INTRODUCTION

Dynamical relaxation processes near massive black holes (MBH) in galactic centers affect the rates of strong stellar interactions with the MBH, such as tidal disruption, tidal dissipation, or gravitational wave (GW) emission (e.g. Alexander 2005). These relaxation processes may also be reflected by the dynamical properties of the different stellar populations there (Hopman & Alexander 2006), as observed in the Galactic Center (Genzel et al. 2000; Paumard et al. 2006). Of particular importance, in anticipation of the planned Laser Interferometer Space Antenna (LISA) GW detector, is to understand the role of relaxation in regulating the rate of GW emission events from compact remnants undergoing quasi-periodic extreme mass ratio inspiral (EMRI) into MBHs.

Two-body relaxation, or non-coherent relaxation (NR), is inherent to any discrete large- N system, due to the cumulative effect of uncorrelated two-body encounters. These cause the orbital energy E and the angular momentum J to change in a random-walk fashion ($\propto \sqrt{t}$) on the typically long NR timescale T_{NR} . In contrast, when the gravitational potential has approximate symmetries that restrict orbital evolution (e.g. fixed ellipses in a Keplerian potential; fixed orbital planes in a spherical potential), the perturbations on a test star are no longer random, but correlated, leading to coherent ($\propto t$) torquing of J on short timescales, while the symmetries hold. Over longer times, this results in resonant relaxation (RR) (Rauch & Tremaine 1996; Rauch & Ingalls 1998; §2.2), a rapid random walk of J on the typically short RR timescale $T_{\text{RR}} \ll T_{\text{NR}}$. RR in a near-Keplerian potential can change both the direction and magnitude of \mathbf{J} (“scalar RR”), thereby driving stars to near-radial orbits that interact strongly with the MBH. RR in a near-spherical potential can only change the direction of \mathbf{J} (“vector RR”).

RR is particularly relevant in the potential near a MBH, where compact EMRI candidates originate.

Hopman & Alexander (2006) show that RR dominates EMRI source dynamics. Depending on its still poorly-determined efficiency, RR can either increase the EMRI rate over that predicted assuming NR only, or if too efficient, it can strongly suppress the EMRI rate by throwing the compact remnants into infall (plunge) orbits (cf Fig. 6 below) that emit a single, non-periodic and hard to detect GW burst. A prime motivation for the systematic numerical investigation of RR efficiency presented here, are the still open questions about the implications of RR for EMRI rates and orbital properties.

This paper is organized as follows. In §2 we briefly review the theory of NR and RR relaxation and derive a new relation between scalar and vector RR. In §3 we describe our method of analyzing and quantifying the effects of RR in N -body simulations, which are described in §4. We present our results in §5 and discuss and summarize them in §6.

2. THEORY

2.1. Non-coherent Relaxation (NR)

The NR time for E -relaxation, T_{NR}^E , corresponds to the time it takes non-coherent 2-body interactions to change the stellar orbital energy by order of itself, $|\Delta E| \sim E$ (by stellar dynamical definition convention, $E > 0$ for a bound orbit). Similarly, the NR time for J -relaxation, T_{NR}^J , corresponds to the time it takes the stellar orbital angular momentum to change by order of the circular angular momentum $|\Delta J| \sim J_c$, where near a MBH of mass M , $J_c = GM/\sqrt{2E}$. The E -relaxation timescale can be estimated by considering the rate Γ of gravitational collisions in a system of size R at a relative velocity v , between a test star and N field stars of mass m and space density $n \sim N/R^3$, at the minimal impact parameter where the small angle deflection assumption still holds, $r_{\text{min}} \sim Gm/v^2$. The collision rate is then $\Gamma \sim nvr_{\text{min}}^2 \sim G^2m^2n/v^3$. Taking into account also collisions at larger impact parameters increases the rate by the Coulomb logarithm factor $\ln \Lambda \sim \ln(R/r_{\text{min}})$. Therefore, $T_{\text{NR}}^E \sim v^3/(G^2m^2n \ln \Lambda)$. Near the MBH $v^2 \sim GM/R$, and so $\ln \Lambda \sim \ln Q$, where $Q \equiv M/m$ is the mass ratio.

¹ Present address: Israel Aerospace Industries, MLM Division, PO Box 45, Beer-Yaakov, 70350, Israel

² William Z. and Eda Bess Novick Career Development Chair

When the stars move under the influence of the central MBH ($Q \gg N$), the relaxation time can be expressed as $T_{\text{NR}}^E \sim (M/m)^2 P / (N \ln \Lambda)$, where $P = 2\pi \sqrt{R^3/GM}$ is the Keplerian period. Following the notation of Rauch & Tremaine (1996) (RT96), the NR changes in E , J and \mathbf{J} over the dimensionless time-lag $\tau \equiv (t_2 - t_1)/P_1$ are

$$|\Delta E|/E \equiv |E_2 - E_1|/E_1 = \alpha_\Lambda \sqrt{N}(m/M)\sqrt{\tau}, \quad (1)$$

$$|\Delta J|/J_c \equiv |J_2 - J_1|/J_{c,1} = \eta_{s\Lambda} \sqrt{N}(m/M)\sqrt{\tau}, \quad (2)$$

$$|\Delta \mathbf{J}|/J_c \equiv |\mathbf{J}_2 - \mathbf{J}_1|/J_{c,1} = \eta_{v\Lambda} \sqrt{N}(m/M)\sqrt{\tau}, \quad (3)$$

where $\alpha_\Lambda \equiv \alpha \sqrt{\ln \Lambda}$ and $\eta_{s,v\Lambda} \equiv \eta_{s,v} \sqrt{\ln \Lambda}$ are dimensionless constants, whose exact values are system-dependent and cannot be estimated with accuracy without detailed calculations or simulations. The corresponding NR timescales are related to these coefficients by $T_{\text{NR}}^E = (M/m)^2 P / (N \alpha_\Lambda^2)$, $T_{\text{NR}}^J = (M/m)^2 P / (N \eta_{s\Lambda}^2)$ and $T_{\text{NR}}^{\mathbf{J}} = (M/m)^2 P / (N \eta_{v\Lambda}^2)$.

2.2. Resonant Relaxation (RR)

When the potential has symmetries that restrict the orbital evolution, for example to fixed ellipses in the potential of a point mass, or to planar annuli in a spherical potential, the perturbations on a test star are no longer random, but correlated. This leads to a coherent changes in \mathbf{J} on times $P \ll t < t_\omega$, $\Delta \mathbf{J} = \mathbf{T}t$, by the residual torque $|\mathbf{T}| \sim \sqrt{N}Gm/R$ exerted by the N randomly oriented, orbit-averaged mass distributions of the surrounding stars (mass wires for elliptical orbits in a Kepler potential, mass annuli for rosette-like orbits in a spherical potential). The coherence time t_ω is set by deviations from the true symmetry, which lead to a gradual orbital drift and to the randomization of \mathbf{T} . For example, the enclosed stellar mass leads to non-Keplerian retrograde precession; General Relativity leads to prograde precession. Ultimately, the coherent torques themselves randomize the orbits (alternatively, this can be viewed as the result of potential fluctuations due to the finite number of stars). The effective coherence time is set by the shortest de-coherence (quenching) process in the system. The accumulated change over t_ω , $|\Delta \mathbf{J}_\omega| \sim |\mathbf{T}t_\omega|$, then becomes the basic step-size, or mean free path in \mathbf{J} -space, for the long-term ($t \gg t_\omega$) non-coherent ($\propto \sqrt{t}$) relaxation of \mathbf{J} . Since this step-size is large, RR can be much faster than NR. The RR timescale T_{RR} is then defined by $\Delta J/J_c = (\Delta J_\omega/J_c) \sqrt{t/t_\omega} \equiv \sqrt{t/T_{\text{RR}}}$. Note that the relaxation of E is not affected by RR because the potential of the system is stationary on the coherence timescale, and so E changes incoherently on all time scales. The torques exerted by elliptical mass wires in a Kepler potential can change both the direction and magnitude of \mathbf{J} . In contrast, the torques exerted by planar annuli can only change the direction of \mathbf{J} .

Here we consider only Newtonian dynamics. The coherence timescale for scalar RR is determined by the time it takes for the orbital apsis to precess by angle $\sim \pi$ due to the potential of the enclosed stellar mass (“mass precession”),

$$t_\omega = t_M = A_M (M/Nm) P, \quad (4)$$

where A_M is an $O(1)$ factor reflecting the approximations in this estimate. The coherence timescale for vector RR is determined by the time it takes for the coherent torques to change $\Delta |\mathbf{J}| \sim J_c$ (alternatively, this is the timescale $t_\phi = (\phi/\Delta\phi_\star)P/2$ to accumulate $O(1)$ fluctuations in the

stellar potential $\Delta\phi_\star \sim \sqrt{N}Gm/R$ relative to the total gravitational potential ϕ as the stars rotate by $\sim \pi$ on their orbits),

$$t_\omega = t_\phi = A_\phi \left(\sqrt{N}/2\mu \right) P \simeq \left[A_\phi (M/m) / 2\sqrt{N} \right] P, \quad (5)$$

where A_ϕ is an $O(1)$ factor, $\mu = Nm/(M + Nm)$ and where the approximate equality is for the Keplerian limit $Nm \ll M$. Following RT96, the RR changes in J and \mathbf{J} during the coherent phase ($\tau < \tau_\omega$) can be expressed as

$$|\Delta J|/J_c \equiv |J_2 - J_1|/J_{c,1} = \beta_s \sqrt{N}(m/M)\tau, \quad (6)$$

$$|\Delta \mathbf{J}|/J_c \equiv |\mathbf{J}_2 - \mathbf{J}_1|/J_{c,1} = \beta_v \sqrt{N}(m/M)\tau, \quad (7)$$

where the $O(1)$ dimensionless coefficients β_s and β_v depend on the parameters of the system and reflect the uncertainties introduced by the various approximations and simplification of this analysis. Accurate determination of their values requires detailed calculations or simulations.

The scalar RR change ΔJ on time-lags $\tau \gg \tau_M$ is then

$$|\Delta J|/J_c \equiv |J_2 - J_1|/J_{c,1} = \beta_s \sqrt{A_M(m/M)}\sqrt{\tau}, \quad (8)$$

and the scalar RR timescale is

$$T_{\text{RR}}^J = [(M/m)/A_M\beta_s^2] P. \quad (9)$$

The RR efficiency factor $\chi = (\beta_s/\beta_{s,\text{RT96}})^2$ defined by Hopman & Alexander (2006) expresses how much shorter T_{RR}^J is relative to the value estimated by RT96. Scalar RR is faster than NR by a factor $T_{\text{NR}}^J/T_{\text{RR}}^J \propto (M/m)/N \ln \Lambda$. Similarly, the vector RR change $|\Delta \mathbf{J}|$ on time-lags $\tau \gg \tau_\phi$ in the Keplerian limit is

$$|\Delta \mathbf{J}|/J_c \equiv |\mathbf{J}_2 - \mathbf{J}_1|/J_{c,1} = \beta_v \sqrt{\frac{1}{2}A_\phi \sqrt{N}(m/M)}\sqrt{\tau}, \quad (10)$$

and the vector RR timescale is

$$T_{\text{RR}}^{\mathbf{J}} = \left[2(M/m) / \sqrt{N}A_\phi\beta_v^2 \right] P. \quad (11)$$

RT96 performed a limited set of near-Keplerian simulations to check their predictions. They analyzed the results both star by star and in the average and observed the coherent growth of $\Delta J/J_c$ and $|\Delta \mathbf{J}|/J_c$ relative to the simulation’s initial values. Although the evolution of these quantities for any single star was very noisy and the proportionality factors had a very large scatter, RR was clearly observed, as predicted.

2.2.1. Relation between scalar and vector RR

The population averages of the scalar and vector coefficients $\eta_{s,v}$ and $\beta_{s,v}$, are not independent quantities. Rather, $\langle \eta_v \rangle = c \langle \eta_s \rangle$, and $\langle \beta_v \rangle = c \langle \beta_s \rangle$ (on timescales $t < t_\omega$), where the constant c depends on the averaging procedure. Here we average $|\Delta \mathbf{J}|(\tau)$ and $\Delta J(\tau)$ by the rms over the stellar population (§3). We focus on the limit where $|\Delta \mathbf{J}|/J \ll 1$, and assume that the change is isotropic on average, $\langle |\Delta \mathbf{J}|^2 \rangle = 3 \langle |\Delta J_i|^2 \rangle = \delta^2$, ($i = x, y, z$), as is indicated by our simulations (§4). The rms of vector RR is δ . Defining the z -axis along \mathbf{J} , then $\Delta J = \Delta J_z$ in the small change limit, and its

rms is $\delta/\sqrt{3}$. Therefore (see Eqs. 2, 3, 6, 7) $\eta_v = \sqrt{3}\eta_v$ for all τ and $\beta_v = \sqrt{3}\beta_s$ for $\tau \ll \tau_M, \tau_\phi$, as is indeed seen in the simulations³ (Fig. 2).

The constant ratio between the population averages of the vector and scalar coefficients is in part a geometrical effect (1D vs 3D changes) and in part a reflection of the symmetries of the perturbations (isotropic $\Delta\mathbf{J}$). This strict proportionality is not expected to hold when $|\Delta\mathbf{J}|/J \sim 1$, for example when only very eccentric stars ($J \rightarrow 0$) are included in the sample, or for very long time-lags.

3. RR DETECTION BY AUTO-CORRELATION ANALYSIS

Given the high computational cost of the N -body simulations, and the very large variance in the evolution of individual orbits, it is essential to extract the RR signal as efficiently and robustly as possible from the simulated data. After some experimentation, we adopted the auto-correlation analysis for detecting and measuring RR in N -body simulation snapshots. Our procedure is as follows.

(1) The stellar phase space coordinates are transformed to the rest-frame of the MBH, which is almost identical with the center of mass in the near-Keplerian system close to the MBH.

(2) The energy ($E_i^{(n)}$), angular momentum ($\mathbf{J}_i^{(n)}$), circular angular momentum ($J_{c,i}^{(n)}$) and Keplerian period ($P_i^{(n)}$) are calculated for the n 'th star ($n = 1 \dots N$) at discrete times t_i in the simulation ("snapshots").

(3) To make full use of the data, we assign a normalized time-lag $\tau_{ji}^{(n)} = (t_j - t_i)/P_i^{(n)}$ for each pair of times ($t_j > t_i$). For each of the N stars, we calculate the normalized energy and angular momentum differences at all lags, $(\Delta E/E)_{ji}^{(n)} = (E_j^{(n)} - E_i^{(n)})/E_i^{(n)}$, $(\Delta J/J_c)_{ji}^{(n)} = (J_j^{(n)} - J_i^{(n)})/J_{c,i}^{(n)}$ and $(\Delta \mathbf{J}/J_c)_{ji}^{(n)} = |\mathbf{J}_j^{(n)} - \mathbf{J}_i^{(n)}|/J_{c,i}^{(n)}$.

(4) The differences from all stars are binned into discrete τ -bins according to their associated τ_{ij} . The bin rms values and their standard deviations are calculated and plotted against the bin's average time-lag $\tau = \langle \tau_{ij} \rangle$, thereby creating the auto-correlation curve.

By using all possible time-lags recorded in the simulation, this approach makes maximal use of the entire data set and averages over the strongly fluctuating individual relaxation curves (cf the RT96 procedure, §2.2). However, this method is not entirely free of bin-to-bin bias. Since the number of orbital periods completed by a star with a mean period $P_i^{(n)}$ over the simulation time t_{sim} is $t_{\text{sim}}/P_i^{(n)} = \tau_{\text{max}}^{(n)}$, long-period stars will not contribute to a high- τ bin, $\langle \tau \rangle_i$ if $\tau_{\text{max}}^{(n)} < \langle \tau \rangle_i$. Conversely, short-period stars will not contribute to a low- τ bin, $\langle \tau \rangle_i$, if $\tau_{\text{min}}^{(n)} > \langle \tau \rangle_i$, where $\tau_{\text{min}}^{(n)} = \min_j (t_{j+1} - t_j)/P_i^{(n)}$ is set by the minimal time difference between consecutive snapshots. In extreme cases some stars may not contribute to the relaxation curve at any $\langle \tau \rangle_i$. Since long and short period stars could well have systematically different responses to RR, this introduces bias to the relaxation curve. This bias can be minimized, at the cost of losing some information, by using only the middle range of the τ -bins, or at a computational cost, by longer simulations with a higher snapshot rate.

4. SIMULATIONS

³ It can be shown that if the population's mean absolute difference $\langle |\Delta\mathbf{J}| \rangle$ is used to define $\beta_{s,v}$, then $\beta_v = 2\beta_s$.

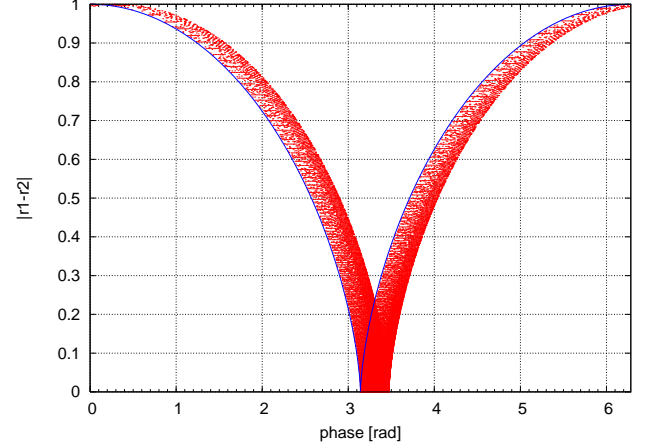


FIG. 1.— Phase drift in a 2-body system over a time of $\tau_{\text{sim}} = 1.35 \times 10^4$ for a $Q = 3 \times 10^{-7}$ mass ratio and an extreme eccentricity of $e = 0.99995$. The line is the initial phase curve (r as function of ψ); the dots are the simulated data. The phase drift of $\Delta\psi = 0.2875$ corresponds to $\tau\Delta\psi \simeq 3.3 \times 10^5$.

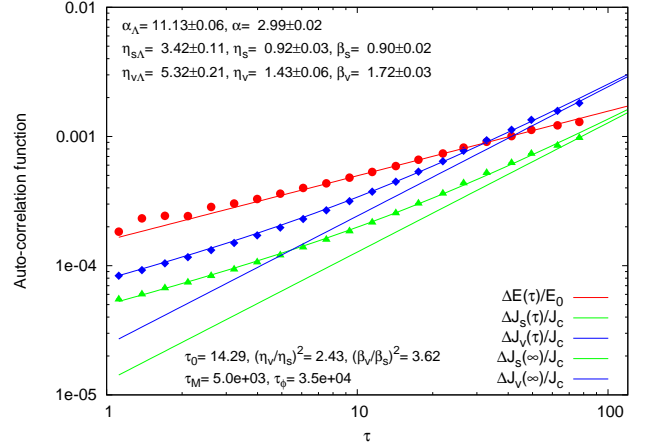


FIG. 2.— The measured (points) and fitted (lines) auto-correlation curves for $\Delta E/E$, $|\Delta J|/J_c$ and $|\Delta \mathbf{J}|/J_c$ in a $Q = 10^6$, $\gamma = 1.5$ simulation with $N = 200$ particles. The points are the results of the N -body simulation, the thick lines are the predicted theoretical curves; the thin straight lines show the asymptotic ($\tau \gg \tau_0$) linear behavior. The best fit parameters and related quantities are also listed.

Our N -body code uses a 5th order Runge-Kutta integrator with individual time-steps and pair-wise K-S regularization (Kustaanheimo & Stiefel 1965), without gravity softening. The time steps were chosen to conserve total energy at the level of $\Delta E_{\text{tot}}/E_{\text{tot}} \sim O(10^{-5}) - O(10^{-8})$, well below the NR energy changes expected in the simulations.

The N -body code must maintain phase coherence to a high enough accuracy to reliably simulate RR. It is thus important to verify that the numerical phase drift in the simulation is much smaller than that due to physical processes, such as mass precession. Experience shows that most of the phase drift $\Delta\psi$ accumulates near periaapse, where the acceleration is largest, and is therefore more pronounced in eccentric orbits. We estimated the phase drift by integrating a highly eccentric ($e = 0.99995$) 2-body system over many orbits, and plotted the relative distance between the 2 masses as function of the orbital phase (Fig. 1), as it evolved during the simulation. The phase spread relative to the theoretical phase curve, $\Delta\psi$, was measured near $\psi = \pi/2$. We define the phase de-coherence

timescale as $\tau_{\Delta\psi} \equiv (\pi/\Delta\psi)\tau_{\text{sim}}$. We estimate conservatively that our near-Keplerian simulation typically have $\tau_{\Delta\psi} > 10^5$ (This is for highly eccentric orbits. We do not detect any phase drift up to $\tau \sim 10^5$ in orbits with moderate eccentricities). Since $\tau_{\Delta\psi} > \tau_w \gg \tau_{\text{sim}}$ for the models simulated here (cf Fig. 2), it can be safely neglected.

Our simulations consisted of 200 particles (including the MBH as a free particle). The initial orbital semi-major axes were randomly drawn from a $\rho(a)da \propto a^{2-\gamma}da$ distribution for $\gamma = 1, 1.5, 1.75$, for a in the range $(0, 1/2)$, with eccentricities drawn from a thermal $\rho(e)de = 2ede$ distribution, with random phases, orbital orientations and isotropic velocities. This distribution corresponds to an $r^{-\gamma}$ number density distribution with an outer cutoff at radius $r = R = 1$ from the MBH (in dimensionless units where $G = 1$, $M + Nm = 1$). These stellar cusps span a wide range of possible physical scenarios (e.g. Bahcall & Wolf 1977), and in particular those of LISA targets, which are expected to be relaxed galactic nuclei (Alexander 2007). A typical simulation lasted a few $\times 100$ system orbital times and resulted in few $\times 100$ snapshots of the system configuration. In order to decrease the statistical errors we ran $n_{\text{sim}} = 5-8$ simulations with different initial conditions for each of the (γ, Q) models we studied.

In Fig. (2) we plot the measured auto-correlation curves in a typical simulation for $\tau \ll \tau_w$: $(\Delta E/E)(\tau)$, $(\Delta J/J_c)(\tau)$ and $(\Delta \mathbf{J}/J_c)(\tau)$. The curves reflect the joint effects of NR and RR. The coefficients $\eta_{s,v}$ and $\beta_{s,v}$ are measured by fitting the auto-correlation curves in the coherent phase to the functions

$$|\Delta J|/J_c = \sqrt{N}(m/M) \sqrt{\eta_{s\Lambda}^2 \tau + \beta_s^2 \tau^2}, \quad (12)$$

$$|\Delta \mathbf{J}|/J_c = \sqrt{N}(m/M) \sqrt{\eta_{v\Lambda}^2 \tau + \beta_v^2 \tau^2}, \quad (13)$$

where the two terms in the square root express the contributions of NR and RR, respectively. Note that on short timescales, $\tau < \tau_0 \equiv (\eta_{s\Lambda}/\beta_s)^2$, the RR auto-correlation curve rises as $\sqrt{\tau}$ due to the effect of NR. It then rises as τ in the RR-dominated coherent phase at times $\tau_0 < \tau < \tau_w$, before turning over again to a $\sqrt{\tau}$ rise in the accelerated random-walk phase at $\tau > \tau_w$ (not shown in Fig. 2). The NR and RR parameters were derived from the best 2-parameter fits of Eqs. (1, 12, 13) to the data. To control the star to star variance, we limited our analysis to time-lag bins that sampled at least 0.75 of the stars in the simulation (§3). The excellent fit of the data points to the predicted auto-correlation curves seen in Fig. (2) indicates that RR is present and measurable.

5. RESULTS

Although the auto-correlation analysis stabilizes against star to star scatter in a single simulation, we still find a large simulation to simulation scatter in the derived values of the coefficients. We therefore constructed a large grid of near-Keplerian models (within the computational time limitations), where RR should be clearly detected.

We summarize our results in table (1) and in Figs. (3, 4, 5). The coefficients α_Λ and $\eta_{s,v\Lambda}$ do not directly express the intrinsic properties of NR, since they should vary as $\sqrt{\ln \Lambda} \simeq \sqrt{\ln Q} \simeq 4(1 \pm 0.07)$ over the Q -range of our models. This small fractional difference and the relatively low statistics of our simulation suite may explain why we do not detect a clear Q -dependence in these quantities. Since we do not see a clear γ or Q dependence, we adopt as the best fit estimates of the values of α , $\eta_{s,v}$ and $\beta_{s,v}$ their grand average over all the

TABLE 1
MEASURED NR AND RR COEFFICIENTS ^a.

γ	Q	n_{sim}	$\bar{\alpha}_\Lambda$	$\bar{\eta}_{s\Lambda}$	$\bar{\eta}_{v\Lambda}$	$\bar{\beta}_s$	$\bar{\beta}_v$
1	10^6	5	10.60 ± 0.58	4.26 ± 0.27	6.56 ± 0.46	1.15 ± 0.10	2.00 ± 0.16
1	10^7	6	10.85 ± 0.91	4.60 ± 0.34	6.82 ± 0.42	1.28 ± 0.13	2.17 ± 0.22
1	10^8	6	11.57 ± 1.52	4.17 ± 0.18	6.18 ± 0.29	1.06 ± 0.09	1.95 ± 0.13
1.5	10^6	5	12.20 ± 1.23	4.03 ± 0.27	6.40 ± 0.42	1.03 ± 0.10	1.76 ± 0.15
1.5	10^7	6	15.63 ± 4.33	4.17 ± 0.33	6.92 ± 0.53	1.02 ± 0.06	1.83 ± 0.08
1.5	10^8	8	19.12 ± 6.05	5.09 ± 0.52	8.43 ± 1.11	1.16 ± 0.11	2.35 ± 0.35
1.75	10^6	6	13.00 ± 1.15	3.95 ± 0.19	6.12 ± 0.39	1.03 ± 0.09	1.93 ± 0.17
1.75	10^7	8	19.61 ± 3.76	4.05 ± 0.53	$6.11\pm.057$	0.97 ± 0.09	1.81 ± 0.15
1.75	10^8	6	16.05 ± 2.31	3.70 ± 0.15	$5.67\pm.017$	0.97 ± 0.07	1.80 ± 0.09
Grand average ^b			$\langle\alpha\rangle$	$\langle\eta_s\rangle$	$\langle\eta_v\rangle$	$\langle\beta_s\rangle$	$\langle\beta_v\rangle$
56			3.65 ± 0.28	1.06 ± 0.03	1.65 ± 0.05	1.07 ± 0.03	1.97 ± 0.07

^a The quoted errors are the errors on the mean (the sample rms is $\sqrt{n_{\text{sim}}}$ times larger).

^b $\langle \alpha \rangle = \langle \alpha_\Lambda / \sqrt{\ln \Lambda} \rangle$, $\langle \eta_{s,v} \rangle = \langle \eta_{s,v\Lambda} / \sqrt{\ln \Lambda} \rangle$ over all simulations for $\Lambda = Q$.

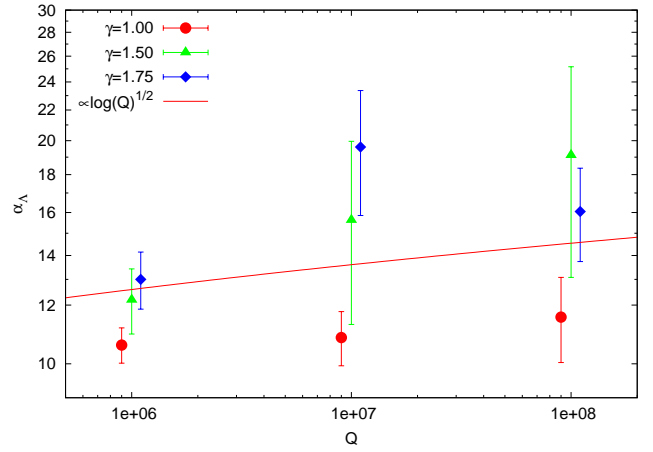


FIG. 3.— Measured NR energy coefficient α_Λ as function of mass ratio Q and for stellar density profiles with logarithmic slopes of $\gamma = 1, 1.5, 1.75$. A $\propto \sqrt{\ln Q}$ curve is shown to guide the eye.

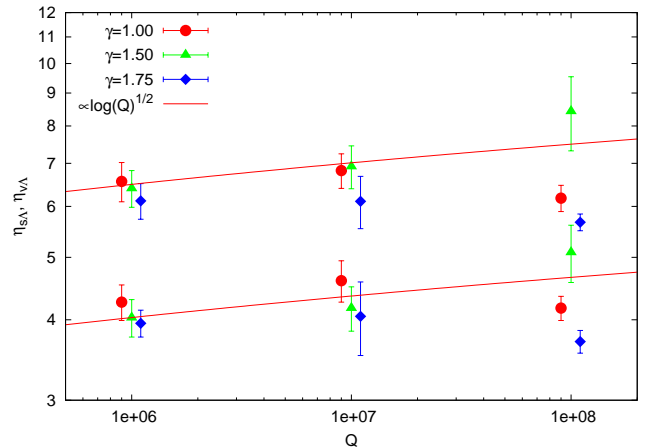


FIG. 4.— Same as Fig. (3), for the measured NR scalar angular momentum coefficient $\eta_{s\Lambda}$ (bottom points) and the vector angular momentum coefficients $\eta_{v\Lambda}$ (top points).

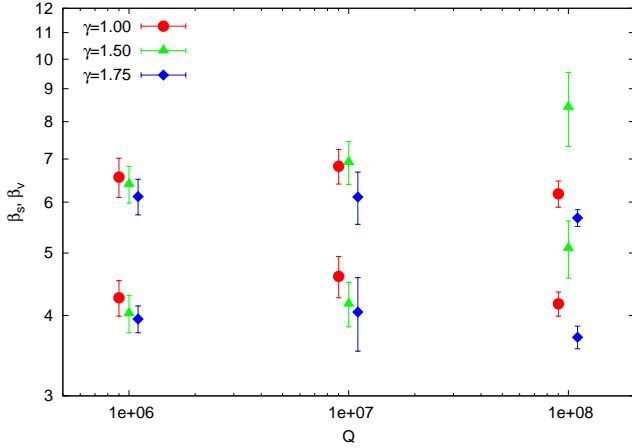


FIG. 5.— Same as Fig. (3), for the measured RR scalar angular momentum coefficient β_s (bottom points) and vector angular momentum coefficient β_v (top points). RR does not depend on a Coulomb factor.

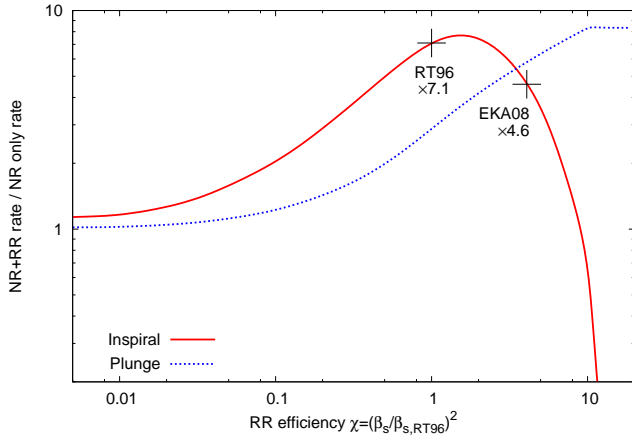


FIG. 6.— The change in the EMRI and plunge rates relative to that predicted assuming only NR, as function of the RR efficiency χ (Adapted from Hopman & Alexander 2006, Fig. 5). The RT96 estimate of β_s ($\chi = 1$) predicts an increase of $\times 7.1$ in the EMRI rate due to RR, close to the maximum. Our (EKA08) new measured efficient RR ($\chi = 4.1$) predicts a higher plunge rate and thus a smaller increase of $\times 4.6$ in the EMRI rate.

simulations (table 1). The measured ratio $\langle \beta_v / \beta_s \rangle = 1.85$ is consistent with the predicted ratio of $\sqrt{3} \simeq 1.73$ (§2.2.1).

RT96 derived from their simulations smaller mean values for β_s (0.53, as compared to 1.07 here) and for α_Λ and $\eta_{s\Lambda}$ (3.09 and 1.37 as compared to 14.76 and 4.25 here). At least part of the difference in α_Λ and $\eta_{s\Lambda}$ can be traced to their use of a softening length $\epsilon = 10^{-2}R \gg Gm/v^2 \sim (m/M)R$ in the calculation of the gravitational force. This decreases the effective value of the Coulomb factor, since $\Lambda \sim R / \max(\epsilon, Gm/v^2) = 10^2$ and so $\sqrt{\ln \Lambda} \simeq 2.1$, about twice as small as in our simulations. Indeed, RT96 noted that decreasing the softening length to $\epsilon = 10^{-4}R$ led to an increased value of $\alpha_\Lambda = 5.5 \pm 0.2$.

It is difficult to trace the specific reason for the discrepancy between our best estimate value for β_s and that derived by RT96, given the many differences in both the simulations and the methods of analysis. Our statistics are better due to the

larger number of simulations and more efficient use of the data, and the analysis here is more rigorous. We therefore briefly consider the implications of this revised value of β_s for EMRI rates. Hopman & Alexander (2006) parametrized the RR efficiency by a factor $\chi = [\beta_s / \beta_{s,RT96}]^2$, and derived the χ dependence of the branching ratio of the EMRI and infall (plunge) rates (Fig. 6). The RT96 value $\chi = 1$ happens to lie very close to the maximum of the RR-accelerated EMRI rate. We find here $\beta_s / \beta_{s,RT96} \sim 2$, which corresponds to a factor ~ 5 increase in the EMRI rate compared to that estimated for NR only, but is a factor ~ 1.5 smaller than implied by the RT96 value, because the higher RR efficiency leads to a higher plunge rate at the expense of the inspiral rate.

6. DISCUSSION AND SUMMARY

We characterized and measured the mean efficiency coefficients of NR ($\alpha_\Lambda, \eta_{s\Lambda}, \eta_{v,\Lambda}$) and RR (β_s, β_v) in Newtonian N -body simulations of isotropic, thermal, near-Keplerian stellar cusps around a MBH. We derived a simple analytical form for the rms RR auto-correlation curves of \mathbf{J} and \hat{J} , and showed that the two are simply proportional to each other. We then measured these coefficients in a large suite of small scale N -body simulations with different stellar density distributions and MBH/star mass ratios. We found no statistically significant trends in the values of these coefficients as function of the system properties. This may require better statistics.

Our measured RR efficiency suggests that RR increases the EMRI rate by a factor of ~ 5 above what is predicted for NR only. This estimate of RR efficiency is consistent with that suggested by the analysis of the dynamical properties of the different stellar populations in the Galactic Center (Hopman & Alexander 2006). However, this conclusion is still preliminary, since several important open issues remain, which should be addressed by larger scale simulations. These include (1) The dependence of the RR coefficients on the orbit of the test star, for example its eccentricity (Gürkan & Hopman 2007). We find that $N \sim 200$ is not enough for reliable statistics on sub-samples within given E or J -bins. The eccentricity dependence of RR is particularly relevant for the supply rate of stars to the MBH from $J \rightarrow 0$ orbits (the loss-cone refilling problem). (2) The effects of a stellar mass spectrum. This will likely affect RR by decreasing the RR timescale, and changing the stellar density distribution through strong mass segregation (Alexander 2007; Alexander & Hopman 2008, in prep.). (3) The robustness of RR against perturbations from the larger non-Keplerian stellar system in which the inner near-Keplerian region of interest is embedded. (4) The role of post-Newtonian effects in RR, such as General Relativistic precession and GW emission. These are expected to play a key role in enabling inspiral by quenching RR just as the compact remnant enters the EMRI phase, and in regulating the GW inspiral rate (Hopman & Alexander 2006).

TA is supported by ISF grant 928/06, ERC Starting Grant 202996-2 and a New Faculty grant by Sir H. Djorgoly, CBE, of London, UK.

REFERENCES

Alexander, T. 2005, Phys. Rep., 419, 65

Alexander, T. 2007, in Black Holes, ed. M. Livio & A. Koekemoer (Cambridge University Press), in press, arXiv:astro-ph/0708.0688

- Bahcall, J. N. & Wolf, R. A. 1977, ApJ, 216, 883
Genzel, R., Pichon, C., Eckart, A., Gerhard, O. E., & Ott, T. 2000, MNRAS, 317, 348
Gürkan, M. A. & Hopman, C. 2007, MNRAS, 379, 1083
Hopman, C. & Alexander, T. 2006, ApJ, 645, 1152
Kustaanheimo, P. & Stiefel, E. 1965, J. Reine Angew. Math., 218, 204
Paumard, T. et al. 2006, ApJ, 643, 1011
Rauch, K. P. & Ingalls, B. 1998, MNRAS, 299, 1231
Rauch, K. P. & Tremaine, S. 1996, New Astronomy, 1, 149